# Coherent Driver Modulator With Flexible Printed Circuit RF Interface for 128-Gbaud Operations

Josuke Ozaki, Yoshihiro Ogiso, *Member, IEEE*, Yasuaki Hashizume, Hiroshi Yamazaki, *Member, IEEE*, Kazuya Nagashima, *Member, IEEE*, and Mitsuteru Ishikawa, *Member, IEEE*

***Abstract*— We developed a flexible printed circuit (FPC) RF interface InP-based high-bandwidth coherent driver modulator (CDM) for 128-Gbaud class operations. To increase the bandwidth of the CDM, an FPC RF interface was introduced to the CDM package, which significantly improved the roll-off frequency by about 40 GHz compared with a conventional package with a surface-mount-type RF interface. The FPC package has a 3-dB bandwidth of about 75 GHz and roll-off frequency above 110 GHz. These are the best characteristics among the CDM packages reported so far. By integrating a modulator with an electro-optic (EO) 3-dB bandwidth of >67 GHz and a driver IC with an electrical 3-dB bandwidth of >75 GHz in this package, the CDM had an EO 3-dB bandwidth of >72 GHz. This EO 3-dB bandwidth is sufficient for 128 Gbaud-class operations. Furthermore, we performed 128-Gbaud dual polarization 16QAM modulations and confirmed good back-to-back bit-error-rate characteristics.**

***Index Terms*— Electro-optic modulation, indium compounds, digital coherent, quadrature amplitude modulation, SiGe BiCMOS technology, flexible printed circuit.**

## I. Introduction

HIGH baud-rates and high multi-level modulation formats are important for increasing the capacity of optical communication systems using digital coherent technology [1], [2]. In particular, a high-bandwidth coherent driver modulator (HB-CDM) [3] is a key component for the optical transmitters of metro and long-haul applications to achieve high speeds and flexible modulation formats. The HB-CDM integrates a driver IC and an optical modulator chip next to each other in one package to reduce RF losses for increasing bandwidth. The CDMs reported to date have a 3-dB bandwidth of over 65 GHz [4], and research and development on higher-bandwidth CDM for over 128-Gbaud-class operations is progressing.

Regarding optical IQ modulator chips that are assembled in the HB-CDM, InP-based IQ modulators have been used for their superior material properties that enable them to achieve high speeds and low driving voltages with a small footprint [4], [5]. An InP IQ modulator with 3-dB electro-optic (EO) bandwidth of 80 GHz and half-wave voltage ($V_\pi$) of 1.5 V has been reported [6]. There are Si modulators and $LiNbO_3$ (LN) modulators using other materials. The 3-dB EO bandwidth of Si photonics modulators is limited to up to about 50 GHz and the $V_\pi$ exceeds 8 V [7], which are not sufficient for high-speed operations. Two types of high-speed thin-film LN (TFLN) modulators have been proposed: one is fabricated on a quartz substrate and the other is fabricated on a Si substrate. A TFLN modulator fabricated on a quartz shows excellent performance with a 3-dB EO bandwidth of over 100 GHz and a $V_\pi$ of 1 V [8]. However, this modulator is too large to be applied to a small form factor such as a HB-CDM. TFLN modulators fabricated on Si have stronger optical confinement, resulting in a smaller chip size with both a 3-dB bandwidth of over 67 GHz and a $V_\pi$ of around 2.5 V [9], [10]. Moreover, a HB-CDM using TFLN modulators on Si has been reported [11]. However, these modulators have a single-ended configuration [12], which is inferior to differential drive modulators in terms of cooperative design and efficient connection with driver ICs [13].

The RF packages reported so far for HB-CDMs have surface-mount-type (SMT) RF interfaces. This is because the SMT configuration is preferred for ease of handling such as in solder mounting. However, the SMT packages have lead pins, and a large impedance mismatch occurs in the connection area between the lead pins and the package ceramics. This limits the roll-off frequency of the SMT package to around 70 GHz [14].

In this letter, we report an InP-based HB-CDM with flexible printed circuit (FPC) RF interface. S-parameter measurements confirmed the FPC package to have a roll-off frequency of over 110 GHz. We used an n-i-p-n heterostructure based twin-IQ modulator, which has low-loss characteristics in both RF and optical aspects. The modulator has a differential capacitively loaded traveling-wave electrode (CL-TWE) structure to achieve efficient connection with a 4-channel linear differential SiGe BiCMOS driver IC with an open-collector output. The HB-CDM has a 3-dB EO bandwidth of over 72 GHz and

Manuscript received 7 August 2022; revised 16 September 2022; accepted 3 October 2022. Date of publication 6 October 2022; date of current version 21 October 2022. *(Corresponding author: Josuke Ozaki.)*

Josuke Ozaki, Yoshihiro Ogiso, Yasuaki Hashizume, and Mitsuteru Ishikawa are with the NTT Device Innovation Center, Nippon Telegraph and Telephone Corporation, Atsugi, Kanagawa 243-0198, Japan (e-mail: josuke.ozaki.mp@hco.ntt.co.jp; yoshihiro.ogiso.uv@hco.ntt.co.jp; yasuaki.hashizume.ph@hco.ntt.co.jp; mitsuteru.ishikawa.pe@hco.ntt.co.jp).

Hiroshi Yamazaki is with NTT Device Technology Laboratories, Nippon Telegraph and Telephone Corporation, Atsugi, Kanagawa 243-0198, Japan (e-mail: hiroshi.yamazaki.mt@hco.ntt.co.jp).

Kazuya Nagashima is with the Advanced Photonic Integrated Devices Development Department, Furukawa Electric Company Ltd., Ichihara, Chiba 290-8555, Japan (e-mail: kazuya6.nagashima@furukawaelectric.com).

Color versions of one or more figures in this letter are available at https://doi.org/10.1109/LPT.2022.3212678.

Digital Object Identifier 10.1109/LPT.2022.3212678

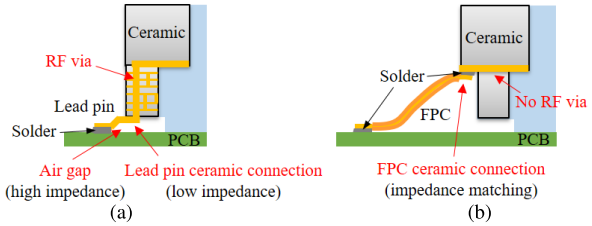


Fig. 1. Schematic diagram of the package structure with (a) SMT and (b) FPC RF interface.

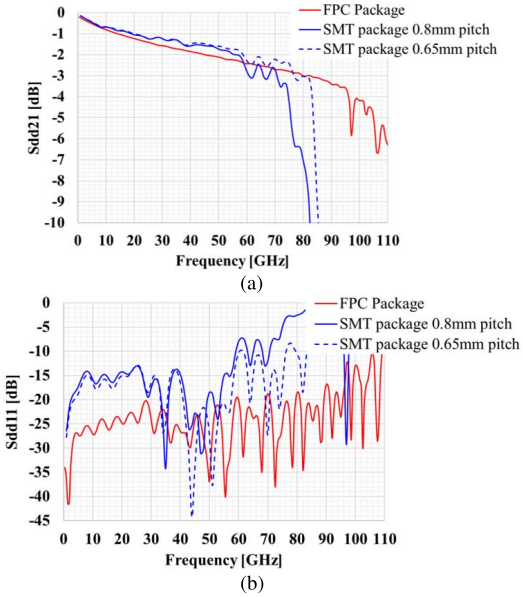


Fig. 2. (a) Sdd21 and (b) Sdd11 simulation results of the SMT and FPC package.

had a bit error rate (BER) of $2.2 \times 10^{-3}$ in an experiment on back-to-back 128-Gbaud dual-polarization (DP) 16 quadrature amplitude modulation (QAM).

## II. Package Configuration

Figure 1 (a) and (b) are simplified schematic diagrams showing the difference in RF interface structure between the SMT package and the FPC package for the HB-CDM. The lead pins and FPC are soldered to the PCB. The SMT package requires RF signal vias to draw RF signals from the lead pins into the package. The smaller the RF via diameter, the higher the roll-off frequency. However, manufacturing restrictions on the RF via diameter limit the RF characteristics. Furthermore, the RF bandwidth is also limited by impedance mismatches in two areas: high impedance due to gaps near the printed circuit board (PCB) contact area caused by the bent structure of the lead pins and low impedance at the connection between the ceramic package and the lead pins.

Figure 2 shows the S-parameter simulation results comparing Sdd21 and Sdd11 of the SMT and FPC packages including the soldering connection area. The FPC package simulation model had a channel pitch of 2.4 mm, the signal-to-signal pad pitch of 0.45 mm, the PCB length (from the FPC connection) of 2.5 mm, and the FPC length of 15 mm. The same channel pitch and PCB length were used for the SMT model, and the two different signal-to-signal lead pitches (0.8 mm and 0.65 mm) were simulated. The Sdd21 results

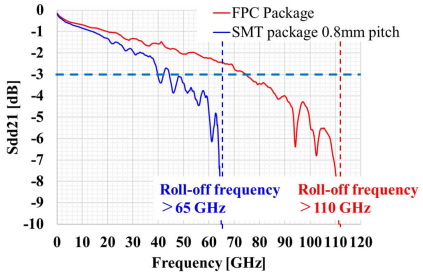


Fig. 3. S-parameter measurement results of the SMT and FPC package.

confirmed the roll-off frequency is improved by reducing the lead pitch from 0.8 mm to 0.65 mm. Even then, the roll-off frequency is still limited to around 80 GHz. In addition, there are manufacturing issues such as the fact that reducing the pitch between the lead pins degrades the mechanical strength of the lead pins. On the other hand, the FPC package does not require RF vias and does not have a large impedance mismatch at each connection surface. Therefore, the Sdd11 of the FPC package is lower than the SMT package. This means that the FPC has better impedance matching. If the lead pins are not bent to a minimum, an air gap is created between the lead pins and the PCB, resulting in a large impedance mismatch. In contrast, FPCs are stable RF transmission lines, so that the impedance mismatch is sufficiently small even if they are bent with a small bending radius. Therefore, unlike lead pins, FPCs can be bent flexibly, eliminating the need for PADs for RF connections on the ceramic surface near the PCB as well as the need for the RF vias. Thus, the FPC package is superior in terms of RF characteristics.

Figure 3 shows the results of S-parameter measurement on the SMT (blue) and FPC package (red). The SMT package has a ground-signal-signal-ground (GSSG) lead configuration with a lead pitch of 0.8 mm and the lead pins were soldered to the PCB for the RF measurement. The results for the SMT package include the PCB length of 2.5 mm from the lead tip [14]. The SMT package has a roll-off frequency around 65 GHz. The S-parameter measurements of the FPC package confirmed that it has a roll-off frequency of over 110 GHz; this is more than 40 GHz higher than that of the measured SMT packages. The FPC has a double-sided FPC structure with a 50 $\mu$m-thick polyimide-based core and 12.5 um-thick polyimide-based coverlay films on both sides. Both the length and width of the FPC are approximately 10 mm. The results do not include the PCB characteristics because the measurements were carried out by directly probing to the FPC. There is a ripple around 100 GHz, but it can be reduced by using smaller-diameter ground vias. This FPC package has a roll-off frequency of over 110 GHz and the potential to support 200-Gbaud class operations.

## III. High-Bandwidth CDM Design

Figure 4 shows the fabricated HB-CDM with the FPC RF interface. The package size is $12 \times 30 \times 5.3$ mm$^3$and the DC interface is based on the SMT configuration. The FPC is made of polyimide and has a length of 10 mm or less. A differential InP-based twin IQ modulator chip based on an n-i-p-n heterostructure [6] and a 4-channel SiGe BiCMOS

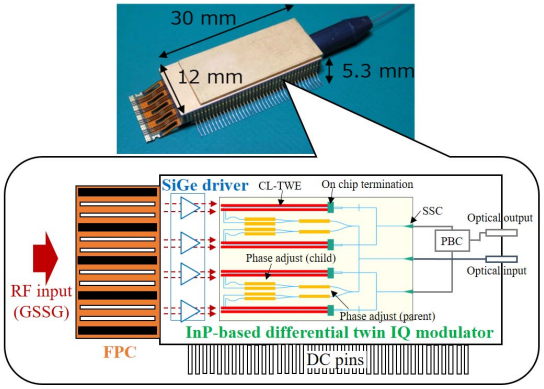


Fig. 4. Photograph and schematic diagram of the fabricated HB-CDM.

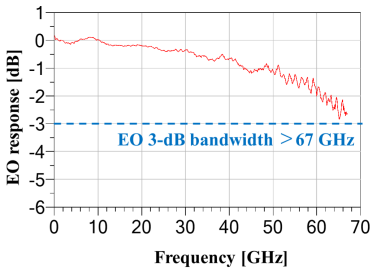


Fig. 5. EO response of the modulator chip standardized at 1 GHz.

differential linear driver IC are assembled together in the package. The modulator chip is mounted on a thermoelectric cooler to maintain a constant operating temperature.

Now, let us describe the structure of the modulator in detail. A spot size converter (SSC) is integrated at the optical input and output ports of the modulator chip. A thermo-optic (TO) heater is used as a phase controller for both child and parent Mach-Zehnder interferometers (MZI). By employing the heater, only the RF area has to have an n-i-p-n structure; the top n-layer can be removed from the other area. This helps to reduce the optical propagation loss. Moreover, the n-i-p-n structure has a thinner p-doped cladding layer and it leads to lower optical and RF propagation loss in the RF region compared with the conventional p-i-n structure. As a result, the on-chip optical loss (excluding the coupling loss) at maximum transmission for each polarization was less than 6.0 dB over the C-band, which is an excellent characteristic. Regarding the RF design of the modulator, a differential CL-TWE structure is used and on-chip RF termination resistors are integrated at the output of the RF electrodes. The characteristic impedance was designed to be 60 Ω, which was determined by co-designing with the driver IC. The EO 3-dB bandwidth of the modulator chip is more than 67 GHz (Fig. 5), and $V_\pi$ is below 2 V.

Regarding the driver IC, an open-collector configuration is used to achieve both high bandwidth and low power consumption [15]. The differential output amplitude is more than 2 $V_{ppd}$ with 60-Ω differential output load resistance, and the power dissipation is less than 3 W. The measured results for Sdd21 of the driver IC are shown in the Fig. 6. These results were re-calculated with the input and output port impedance set to differential 100 Ω and 60 Ω, respectively. Moreover, an inductance of 100 pH was added to the input

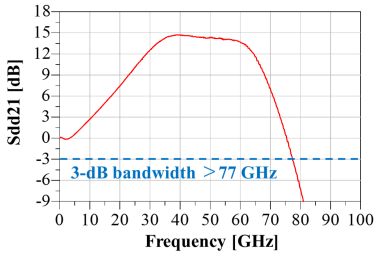


Fig. 6. Sdd21 of the driver IC.

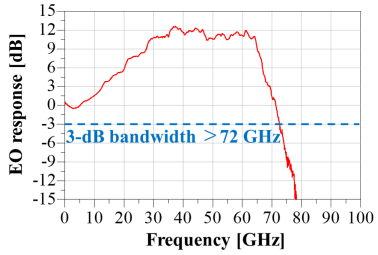


Fig. 7. Small-signal EO response of the HB-CDM standardized at 1 GHz.

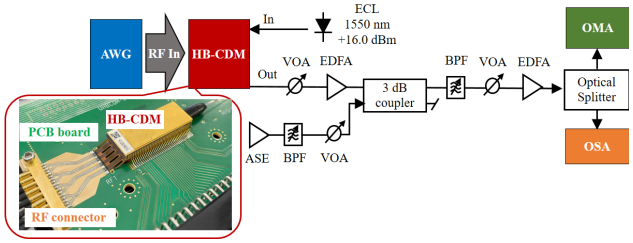


Fig. 8. Experimental setup for back-to-back IQ modulations.

and output ports of the driver, assuming a connecting wire between the package and the driver and between the driver and the modulator. As shown in the graph, the electrical 3-dB bandwidth is over 75 GHz under conditions that take into account the assembly.

## IV. Experimental Results

Figure 7 shows the measured small-signal EO response at 1550 nm for the fabricated CDM soldered to a PCB (Fig. 8). This result includes RF losses on the PCB 2.5 mm from the edge of the FPC and PCB connection area. Transmission line and RF connector losses on the PCB were de-embedded by using a test coupon. The 3-dB EO bandwidth was over 72 GHz. Moreover, the amount of peaking was about 12 dB at 60 GHz relative to 1 GHz. The peaking amount may seem too large for the CDM alone; however, it is designed to compensate for the electrical losses of other components when the CDM is connected to a digital signal processor. In this assembly, the inductance of the wires between the driver and the modulator, which affects the RF characteristics, is estimated to be about 100 pH. The bandwidth and roll-off frequency of the CDM is mainly determined by the RF characteristics of the driver IC. Therefore, the improvement in Sdd21 of the driver IC is the most important factor for further bandwidth expansion. Regarding the other important characteristics of the CDM, the insertion loss (IL) per polarization at the maximum transmission is 8.7 dB for X polarization

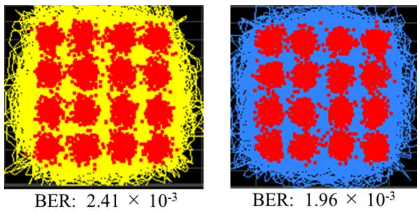


Fig. 9. Constellation diagrams of 128-Gbaud DP-16QAM at best OSNR.

and 8.6 for Y polarization at 1550 nm. The extinction ratio (ER) of child and parent MZIs at 1550 nm are >29 dB and >40 dB, respectively. The optical loss is the lowest among the CDMs reported so far, and the extinction ratio is sufficient for higher-order modulation formats.

The experimental setup for back-to-back IQ modulations is shown in Fig. 8. An external cavity laser (ECL) with a <100 kHz linewidth was used; the output power was +16 dBm and the wavelength was 1550 nm. The RF signal source was a 256 GS/s arbitrary waveform generator (AWG) with a DAC having a 3-dB analog bandwidth of up to 70 GHz, and an optical modulation analyzer (OMA) with a 3-dB analog bandwidth of >100 GHz was used for signal characterization. The RF signals w ere input by connecting the AWG and the PCB via an RF cable, in total about 25-cm long. An erbium-doped fiber amplifier (EDFA) and a variable optical attenuator (VOA) were used to adjust the optical signal power to a constant value. An amplified spontaneous emission (ASE) noise source and a 5.5-nm band-pass filter (BPF) were used to control the received OSNR. The optical output spectrum through a 3-nm BPF was measured by an optical spectrum analyzer (OSA) for the OSNR measurements.

Figure 9 shows the constellations and the BER performance of back-to-back 128-Gbaud DP-16QAM operations at an OSNR of around 42 dB (best OSNR). The OSNR was measured in a 0.1-nm reference noise bandwidth. The RF signals from the AWG were pulse-shaped using a root-raised-cosine (RRC) filter, and the roll-off factor and PRBS were 0.1 and $2^{15-1}$, respectively. The modulator bias was set to obtain a $V_\pi$ of 2.0 V, and the differential gain of the driver at 1 GHz was adjusted to about 12 dB so that modulation depth would be 30%. The modulation loss calculated from the optical output power was about 15 dB in the settings. We confirmed a very clear constellation of 128-Gbaud DP-16QAM with BERs of $2.41 \times 10^{-3}$ for X-polarization and $1.96 \times 10^{-3}$ for Y-polarization at best OSNR. In addition, we have confirmed that the OSNR giving the BERs of $2.0 \times 10^{-2}$ (the pre-FEC BER threshold) is about 26 dB. These results confirm that the bandwidth and other characteristics of the CDM are sufficient for 128-Gbaud-class operations.

## V. Conclusion

We developed an InP-based high-bandwidth coherent driver modulator with an FPC RF interface. By changing the RF interface of the package from the SMT to FPC configuration, the roll-off frequency was increased to above 110 GHz. In addition, by integrating a modulator with a 3-dB EO bandwidth greater than 67 GHz and a driver IC with a 3-dB electrical bandwidth greater than 80 GHz in the FPC package, a CDM with a 3-dB EO bandwidth of more than 72 GHz was achieved. Sufficient RF and optical characteristics resulted in good BER characteristics for 128-Gbaud DP-16QAM operations. The HB-CDM will be employed in pluggable transceivers and for beyond 800-Gb/s per lambda optical transmission systems.

## Acknowledgment

The authors would like to thank to the members of KYOCERA Corporation for support with the RF design, fabrication, and measurement of the FPC package.

## References

[1] K. Kikuchi, "Fundamentals of coherent optical fiber communications," *J. Lightw. Technol.*, vol. 34, no. 1, pp. 157–179, Jun. 1, 2016, doi: 10.1109/JLT.2015.2463719.

[2] K. Roberts, Q. Zhuge, I. Monga, S. Gareau, and C. Laperle, "Beyond 100 Gb/s: Capacity, flexibility, and network optimization," *J. Opt. Commun. Netw.*, vol. 9, no. 4, pp. C12–C24, Apr. 2017, doi: 10.1364/JOCN.9.000C12.

[3] (Jul. 2021). *Implementation Agreement for the High Bandwidth Coherent Driver Modulator (HB-CDM), IA# OIF-HB-CDM-02.0*. [Online]. Available: https://www.oiforum.com/wp-content/uploads/OIF-HB-CDM-02.0.pdf

[4] Y.-W. Chen et al., "InP CDM and ICR enabled 128 Gbaud/ DP-16 QAM-PS and 120 Gbaud/DP-QPSK long-haul transmission," *IEEE Photon. Technol. Lett.*, vol. 34, no. 9, pp. 471–474, May 1, 2022, doi: 10.1109/LPT.2022.3165484.

[5] J. Ozaki et al., "500-Gb/s/$\lambda$ operation of ultra-low power and low-temperature-dependence InP-based high-bandwidth coherent driver modulator," *J. Lightw. Technol.*, vol. 38, no. 18, pp. 5086–5091, Sep. 15, 2020, doi: 10.1109/JLT.2020.2998466.

[6] Y. Ogiso et al., "80-GHz bandwidth and 1.5-V $V_\pi$ InP-based IQ modulator," *J. Lightw. Technol.*, vol. 38, no. 2, pp. 249–255, Jan. 15, 2020, doi: 10.1109/JLT.2019.2924671.

[7] J. Zhou, J. Wang, L. Zhu, and Q. Zhang, "Silicon photonics for 100 Gbaud," *J. Lightw. Technol.*, vol. 39, no. 4, pp. 857–867, Feb. 15, 2021, doi: 10.1109/JLT.2020.3009952.

[8] M. Xu et al., "Dual-polarization thin-film lithium niobate in-phase quadrature modulators for terabit-per-second transmission," *Optica*, vol. 9, no. 1, pp. 61–62, Jan. 2022, doi: 10.1364/OPTICA.449691.

[9] C. Wang et al., "Integrated lithium niobate electro-optic modulators operating at CMOS-compatible voltages," *Nature*, vol. 562, pp. 101–104, Sep. 2018, doi: 10.1038/s41586-018-0551-y.

[10] H. Li et al., "High performance thin-film lithium niobate MZ modulator ready for massive production," in *Proc. Opt. Fiber Commun. Conf. (OFC)*, San Diego, CA, USA, 2022, pp. 1–3, doi: 10.1364/OFC.2022.M2D.5.

[11] S. Makino, S. Takeuchi, S. Maruyama, M. Doi, Y. Ohmori, and Y. Kubota, "Demonstration of thin-film lithium niobate high-bandwidth coherent driver modulator," in *Proc. Opt. Fiber Commun. Conf. (OFC)*, San Diego, CA, USA, 2022, pp. 1–3, doi: 10.1364/OFC.2022.M1D.2.

[12] M. Zhang et al., "Integrated lithium niobate electro-optic modulators: When performance meets scalability," *Optica*, vol. 8, no. 5, pp. 652–667, 2021, doi: 10.1364/OPTICA.415762.

[13] M. Rausch et al., "A performance comparison of single-ended- and differential driving scheme at 64 Gbit/s QPSK modulation for InP-based IQ-Mach-Zehnder modulators in serial-push-pull configuration," in *Proc. Eur. Conf. Opt. Commun. (ECOC)*, Valencia, Spain, Sep. 2015, pp. 1–3, doi: 10.1109/ECOC.2015.7341728.

[14] J. Ozaki, H. Tanobe, and M. Ishikawa, "Crosstalk reduction between RF input channels of coherent-driver-modulator package by introducing enhanced ground lead structure," *Electron. Lett.*, vol. 56, no. 17, pp. 893–1895, 2020, doi: 10.1049/el.2020.1318.

[15] N. Wolf et al., "Electro-optical co-design to minimize power consumption of a 32 GBd optical IQ-transmitter using InP MZ-modulators," in *Proc. IEEE Compound Semiconductor Integr. Circuit Symp. (CSICS)*, New Orleans, LA, USA, Oct. 2015, pp. 1–4, doi: 10.1109/CSICS.2015.7314499.